Physically Accurate Synthetic Images for Computer Vision System Design

by
Holly E. Rushmeier
Johne´ M. Parker
Kok-Mong Lee

GIT-GVU-91-25
October 1991

Graphics, Visualization & Usability Center

Georgia Institute of Technology
Atlanta GA 30332-0280

Physically Accurate Synthetic Images for Computer Vision System Design

Holly E. Rushmeier[1]
Johné M. Parker[2]
Kok-Meng Lee[3]

The George Woodruff School of Mechanical Engineering
Georgia Institute of Technology
Atlanta, GA 30332-0405 USA
fax: (404)894-8336

[1] email: hr3@hydra.gatech.edu, phone:(404)894-3208

[2] email: gt9233a@hydra.gatech.edu, phone:(404)894-5550

[3] **contact author**, email: kmlee@gtri01.gatech.edu, phone:(404)894-7402

October, 1991

Submitted to Vision Interface 1992

Physically Accurate Synthetic Images for Computer Vision System Design

Abstract

The design of a computer vision system for part presentation is a complex hardware/software problem. In the past, standard renderings of parts available from CAD systems have been used as aids in the design process. However, such standard renderings are very limited because of the simple illumination models they employ. We present preliminary results of a study of the utility of physically accurate synthetic images in the design of vision systems. Physically accurate images can potentially be used both for the hardware lighting and sensing design, as well as for template design for model-based matching for part location. We describe how state-of-the-art computer graphics global illumination algorithms can be used to generate images for the vision problem. We present a comparison of a variety of synthetic images to images captured using the GRIPPS retroreflective vision system under development at Georgia Tech.

keywords: computer graphics, computer vision, global illumination, part presentation, retroreflection, synthetic image generation

Physically Accurate Synthetic Images for Computer Vision System Design

1. Introduction

Designing a computer vision system for determining part location is a complex hardware/software problem (Lee, 1991a.) The final design consists of many components including the selection and placement of light sources to illuminate the part, the selection and placement of the sensing elements used to capture the image of the part and the development of software to determine part location and orientation from the captured image. In this paper we consider the use of physically accurate synthetic images in the design of hardware and software for a low cost computer vision system currently in development at Georgia Tech. Synthetic images can potentially be used to reduce the number of hardware configurations to be built and tested, and can provide insight into efficient image processing algorithms for accurate part location.

Synthetic images are frequently used as an aid in testing image processing algorithms (e.g. Wu et al., 1990.) Usually simple image synthesis algorithms, available with many commercial CAD systems, are used to generate these images. These simple algorithms generally assume idealized (i.e. Lambertian) or nonphysical (i.e. Phong) reflectance models, limited light source models (i.e. parallel or isotropic point light sources) and do not attempt to model true camera optics (an ideal pinhole camera is generally used). Such images can be useful in gaining insight into algorithm performance, but they are extremely limited (Chen and Mulgaonkar, 1991.) They cannot, for example, be used reliably to compare the performance of an algorithm in locating a part for two different configurations of the hardware lighting/camera system.

In the field of computer graphics, attempts to generate "photorealistic" images have resulted in the development of highly accurate methods for calculating illumination. The use of such physically accurate methods in an iterative method for interpreting images has been proposed by Gagalowicz (1990). Other researchers, while maintaining that understanding the illumination problem is important, feel that physically accurate images are too computationally expensive to be of use in a vision system (Cowan, 1991). In this paper we present preliminary results from a study of the utility of highly accurate computer graphics synthetic images in the design of a vision system.

We begin by describing the particular vision system design which we ultimately seek to improve. Next we present the methodology used to compute physically accurate synthetic images. Then we present preliminary results comparing synthetic images generated using various methods to images captured by the existing vision system. We conclude with recommendations for improving the accuracy of the synthetic images and tests that can be performed to evaluate alternative configurations of the vision system.

2. The Computer Vision System

The system under study is the computer vision component of GRIPPS, the Generic Retroreflective Integrated Part-Pickup System. GRIPPS has been developed specifically as a low cost part-pickup system. GRIPPS is described in greater detail in Lee, 1991b, and in Lee et al. 1991. Here we review just the basic vision system design, and specify the parameters which we hope to optimize with the aid of synthetic images.

A diagram of the vision system is shown in Fig. 1. The light sources and camera used to illuminate and image the parts are mounted a distance D above a flat horizontal surface on which the parts will be placed. To obtain high contrast between the parts and the background, the horizontal surface is covered with a retroreflective coating. The retroreflective surface has the property that the peak of reflected light energy is in the direction of the incident light, as shown in Fig. 2. When a sensor is collocated with the light source, the radiance reflected by the retroreflective surface is over 300 times that which would be received from a Lambertian surface with a reflectance of $\rho_d = 1$.

To take advantage of the dramatic contrast between the retroreflective background and the part to be located, the camera must be essentially collocated with the light sources used to illuminate the part. In the GRIPPS system, the light sources are a set of N light emitting diodes (LEDs) mounted in a ring of diameter w around a pinhole camera. Each LED emits light in a narrow cone angle ξ. The CCD imaging sensor is located a focal distance f from a pinhole of diameter d. Images are produced by capturing an image for exposure time τ. The signal from the CCD imaging sensor is amplified and electronically sampled through an analog to digital processor, and the resulting array of integer values is sent to an on board digital-signal-processing (DSP) chip.

The design parameters which affect the accuracy of part presentation using computer vision may be broadly divided into two types; namely, the intrinsic and extrinsic parameters. The former characterize the optics f and d, and the illumination w, N, ξ, and D for a specified sensor geometry and field-of-view; and the latter describe the relationship between the camera coordinate frame and the scene coordinate frame (Tsai, 1987). One goal of this ongoing project is to determine the intrinsic parameters that would result in images from which the position and orientation of a wide variety of parts could be obtained more accurately.

The software used to process the image uses a model-based matching approach, described in more detail in Lee and Janakiraman, 1991. The processing begins by identifying the prespecified features such as fiducial marks on the part or simply the sharp curvature on the edge of the part. Features of the part are then matched against that of stored templates of the object. After matching to the template, the location of the center of mass of the object and its orientation can be computed. The template design can be characterized as two distinct

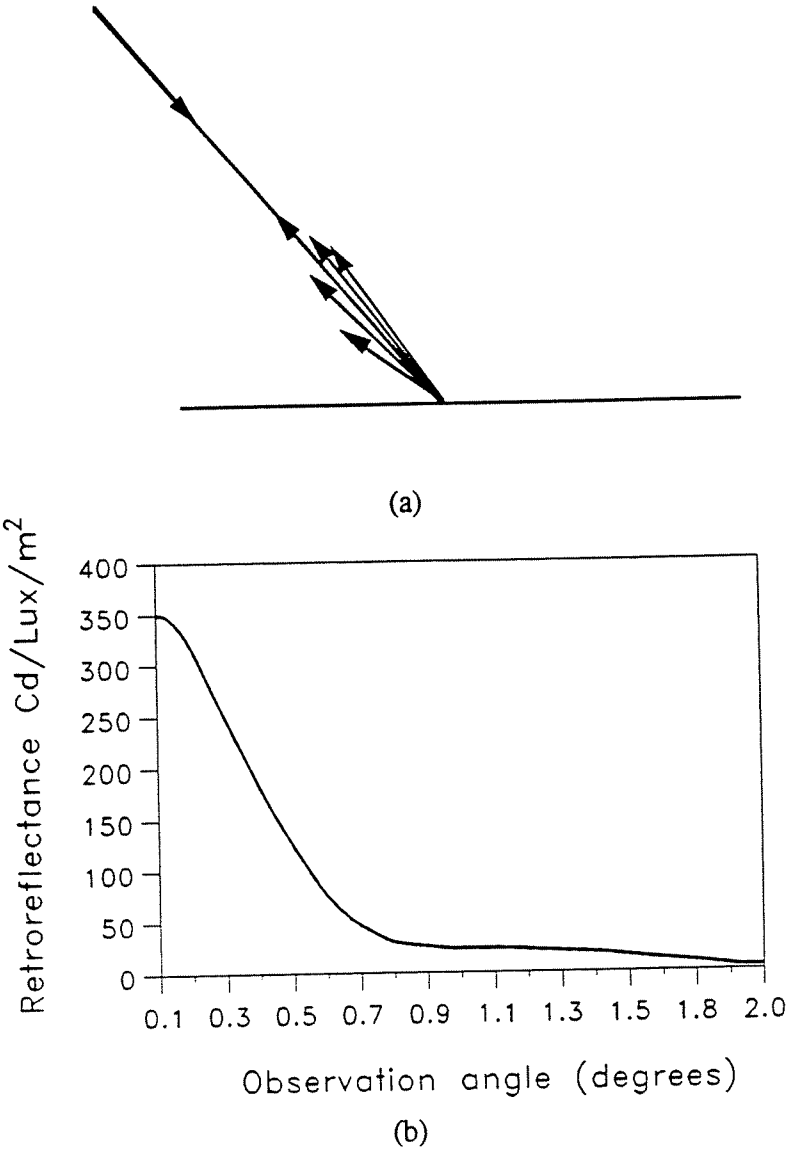

Figure 2: (a) A retroreflective surface reflects most incident energy back into a cone of directions centered around incident direction. (b) A plot of the variation of retroreflectance for normal incidence with the observation angle measured from the surface normal.

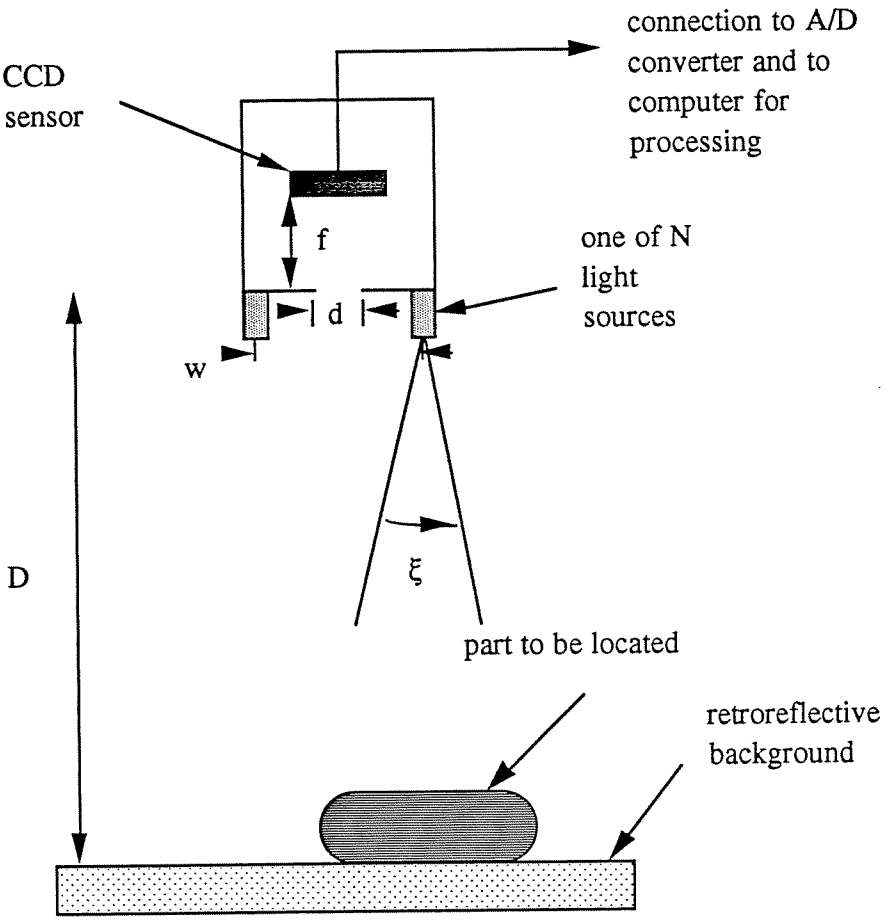

Figure 1: Schematic of vision system showing design parameters.
(Not to scale.)

processes. The first process determines a representation of the geometric charateristics of the parts so that the features can be uniquely and reliably identified in the presence of highlights due to specular reflections introduced by the collocated source or the general ambient lighting. The second process determines an accurate set of geometric data to be used by the image processing software so that the location and orientation of the part can be calculated from the matched features.

A second goal of this project is to develop a template design method using photorealistic CAD representations, taking into account the specific illumination effects (e.g. shadows, specular reflections,etc.) and optic effects (e.g. depth of field, perspective, etc.) which would result when this particular vision system is used.

3. Synthetic Image Generation

In this section we review the basic theory of physically accurate synthetic image generation, and the implementation of a particular image generation system for this project.

3.1 Theory

In computer graphics, the generation of a physically accurate synthetic image has been modelled as a two step process (Meyer et al., 1986), as shown in Fig. 3a. A description of a scene's geometric and optical properties, along with the specification of the viewer position and and image plane is used to simulate the scene illumination, and to determine an array of radiances (i.e. energy/time-projected area- solid angle). These radiances are mapped to the limited dynamic and spectral range of the display monitor. This mapping is specified by a model of human perception (e.g. Tumblin and Rushmeier, 1991) for the computer graphics problem. The output of the perceptual mapping is the array of values of 0-255 to be displayed on the computer monitor.

For the computer vision problem, the process in Fig. 3a must be revised to the process shown in Fig. 3b. The output from the illumination model needs to be energy/area, rather than radiance at each pixel. The mapping based on human perception must be replaced by a model of how the system sensor converts incident light energy into a 0-255 value.

Computer Graphics

To understand how to use computer graphics methods for vision simulations, we begin by looking at the illumination simulation step in the graphics problem. The geometry of the illumination at each image pixel is diagramed in two dimensions in Fig. 4. In most graphics methods, an infinitesimal pinhole is assumed, and a solution is found for the rendering equation (Kajiya, 1986) for each image pixel for each wavelength band:

$$I_{pixel} = \int_{pixel\_area} I_i(\theta_{p,i}, \phi_{p,i}) f(x_p, y_p)\, dA_{pixel} \qquad (1)$$

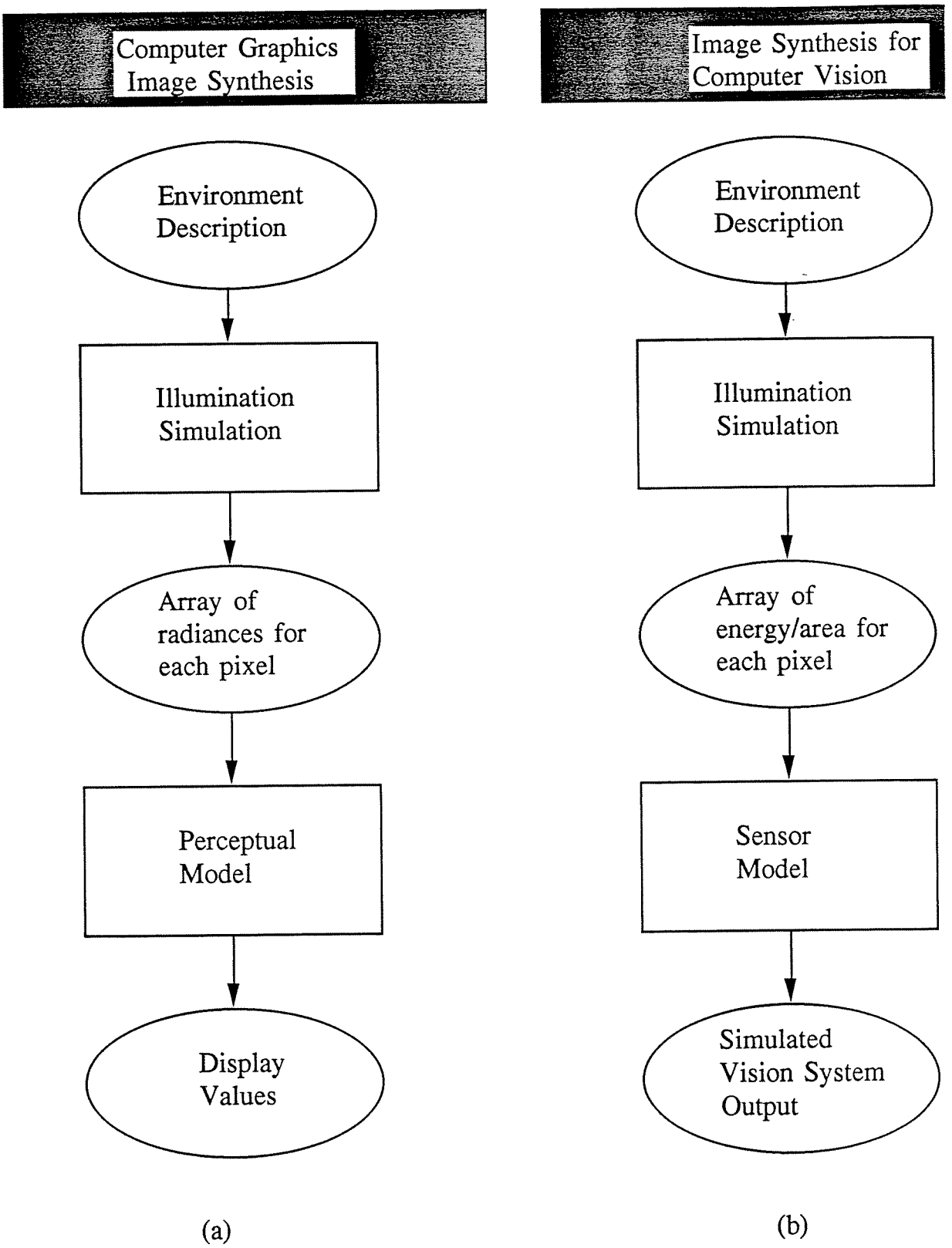

Figure 3: The synthetic image generation process (a) in computer graphics and (b) in computer vision.

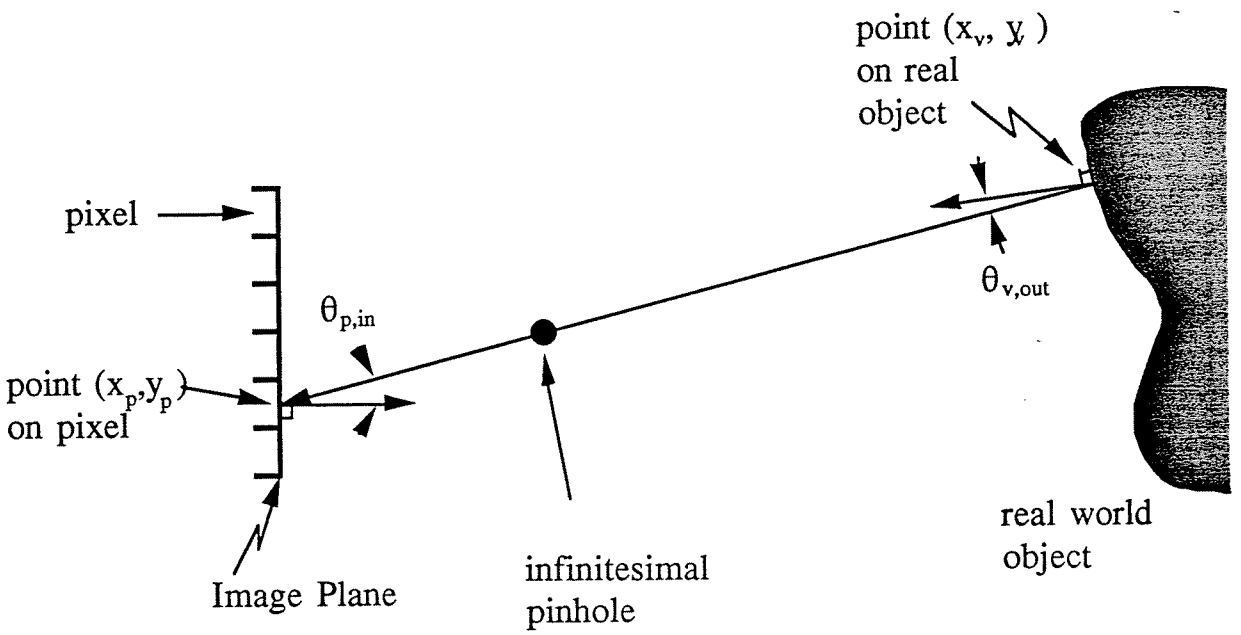

Figure 4: Geometry of image synthesis for an infinitesimal pinhole camera. The radiance incident on a sensor pixel is equal to the radiance leaving the real world object visible from the sensor through the pinhole.

where:

I_{pixel} is the average radiance incident on the pixel, calculated using $f(x_p,y_p)$ as a weighting function over the pixel area, $\int f(x_p,y_p)\, dA_{pixel} = 1$. In the graphics problem the form of $f(x_p,y_p)$ depends on the sensitivity of the human eye.

(x_p,y_p) is a point on the pixel

$I_i(\theta_{p,i},\phi_{p,i})$ is the radiance incident through the infinitesimal pinhole

$(\theta_{p,i},\phi_{p,i})$ is the direction to the infinitesimal pinhole in spherical coordinates based at (x_p,y_p); $\theta_{p,i}$, is the polar angle, $\phi_{p,i}$ is the azimuthal angle

explicit dependence on the wavelength λ is omitted.

Assuming the geometric optics approximation is valid, the value of $I_i(\theta_{p,i},\phi_{p,i})$ is equal to the value of the radiance $I_o(\theta_{v,o},\phi_{v,o})$ for the point (x_v,y_v) on a real object visible along the ray starting at a point on the pixel in the direction $(\theta_{p,i},\phi_{p,i})$. (Note that the bending of rays by diffraction through a small aperture can potentially be accounted for by methods such as described by Nakamae et al., 1990.). For reflective (rather than emitting) surfaces $I_o(\theta_{v,o},\phi_{v,o})$ is not known a priori and must be calculated. As shown in Fig. 5, $I_o(\theta_{v,o},\phi_{v,o})$ depends on the light energy incident on the object. Specifically, $I_o(\theta_{v,o},\phi_{v,o})$ is given by the following equation of radiative transfer (e.g. see Siegel and Howell, 1981):

$$I_o(\theta_{v,o},\phi_{v,o}) = \int_{\cap} \rho_{bd}(\theta_{v,o},\phi_{v,o};\theta_{v,i},\phi_{v,i}) I_i(\theta_{v,i},\phi_{v,i}) \cos\theta_{v,i}\, d\omega_i \qquad (2)$$

where $\rho_{bd}(\theta_{v,o},\phi_{v,o};\theta_{v,i},\phi_{v,i})$ is the bidirectional reflectance of the real world object and the integral is over the entire hemisphere of directions above the real world object at point v.

The incident radiance $I_i(\theta_{v,i},\phi_{v,i})$ may originate at light sources, or may be due to multiple interreflections within the environment. That is, if a light source is visible in direction $(\theta_{v,i},\phi_{v,i})$, the incident radiance is the emitted radiance of the source in the direction of point v. If something other than a light source is visible in direction $(\theta_{v,i},\phi_{v,i})$, the radiance of that object must be calculated by reapplying Eq. (2). In other words, Eq. (2) is recursive for multiple interreflections. Solving Eq. (2) accounts for all possible geometric optic illumination effects -- i.e. shadowing, highlights, caustics, color bleeding, etc.

Methods for efficiently solving Eq. (2) have been studied extensively in computer graphics over the last decade. Radiosity (e.g Goral et al. 1984, Nishita and Nakamae, 1985, Sillion et al. 1991) and Monte Carlo path tracing (e.g. Kajiya 1986, Ward et al. 1988) are the major techniques which have been developed for solving Eq. (2). In radiosity methods the problem is discretized in object space, while in Monte Carlo methods the problem is discretized in image space. Radiosity methods are useful for calculating the overall global

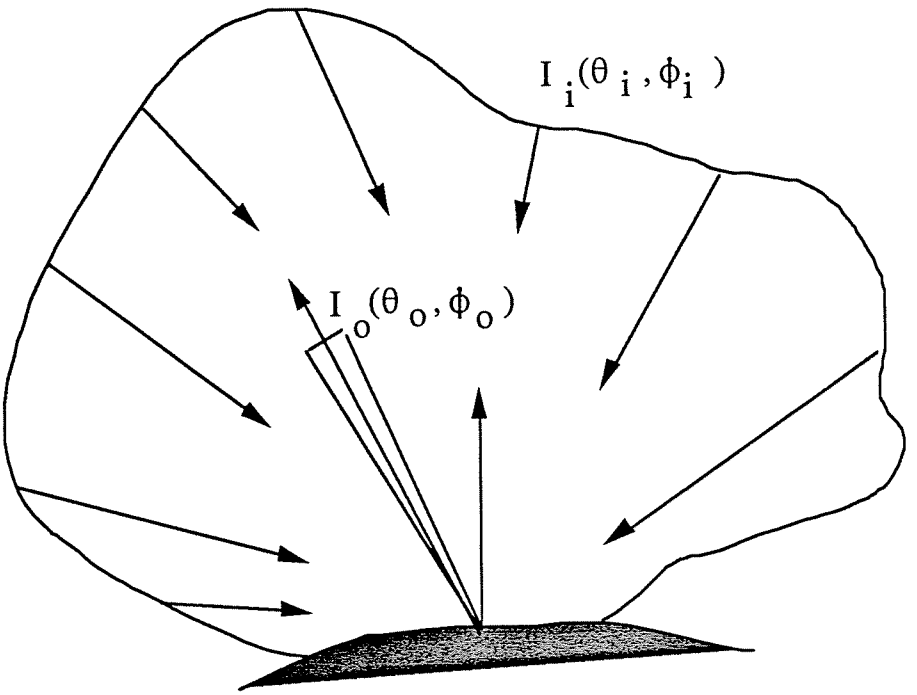

Figure 5: The radiance leaving a surface on a real object in a direction (θo,ϕo) depends on the radiance incident on the surface from all directions. The incident radiance may be from light sources, or may be from secondary reflections off of other surfaces in the environment.

illumination of an environment, while Monte Carlo methods are useful when highly accurate high spatial frequency components of an image are required (Chen et al., 1991).

Computer Vision

For the computer vision problem, the captured image values are related to E_{pixel}, the average *energy /area* incident, not on the average radiance I_{pixel} . To calculate E_{pixel} the size of the finite pinhole in the vision system must be used. E_{pixel} is found by replacing the incident radiance I_{in} in Eq. (1) with the incident energy per unit area E_i:

$$E_{pixel} = \int_{pixel\_area} E_i(\theta_{p,i}, \phi_{p,i}) f(x_p, y_p)\, dA_{pixel} \tag{3}$$

In our work, we assume the spatial sensitivity of each sensor pixel is uniform, and so $f(x_p,y_p)$ is simply $1/A_{pixel}$. $E_i(\theta_{p,i},\phi_{p,i})$ is equal to the integral of the incident radiance times the unit projected area of the pixel in the direction of the pinhole and the sample time τ over the solid angle subtended by the pinhole:

$$E_i(\theta_{p,i}, \phi_{p,i}) = \int_{pinhole} I_i(\theta'_{p,i}, \phi'_{p,i}) \cos\theta'_{p,i}\, \tau\, d\omega_{pinhole} \tag{4}$$

where the direction $(\theta'_{p,i},\phi'_{p,i})$ is in the solid angle subtended by the pinhole, and the center of the pinhole is in direction $(\theta_{p,i},\phi_{p,i})$. As before, the incident radiance $I_i(\theta'_{p,i},\phi'_{p,i})$ is equal to the radiance leaving the visible real world object as given by Eq. (2).

The values E_{pixel} are the appropriate input to the sensor model. Note that although some computer graphics methods have accounted for the depth of field effect resulting from a finite aperture (e.g. Cook et al., 1984), these methods do not calculate E_{pixel}.

The sensor model for a computer vision system is much simpler than the perceptual model based on human vision used in computer graphics image synthesis. Explicitly denoting the spectral dependence of the incident energy per unit area by $E_{pixel}(\lambda)$, the sensor model for the computer vision system can be modelled as a power law:

$$G_{pixel} = K\left(\int_0^\infty E_{pixel}(\lambda) s(\lambda)\, d\lambda\right)^\gamma + G_o \tag{5}$$

where :

G_{pixel} is the output gray scale value,

$s(\lambda)$ is the spectral sensitivity of the sensor

K and γ can are parameters which characterize the camera system

G_o is the background gray scale value

The spectral sensitivity $s(\lambda)$ is given with the manufacturer's data for the sensing element. K and γ need to be calibrated for the system as a whole to account for the non-linear effects of the analog to digital signal conversion, as well as the sensitivity of the sensing element. Equation (5) holds for values of E_{pixel} up to a saturation value $E_{pixel,sat}$, for which G_{pixel} is equal to G_{max}.

3.2 Implementation

Both the graphics problem and the computer vision problem require the solution of the radiative transfer equation given in Eq. (2). Since high spatial frequency variations in illumination are important in the part location problem, a Monte Carlo path tracing approach is more suitable than a radiosity approach. We selected the public domain software package *Radiance* from the Lighting Systems Research Group of the Lawrence Berkeley Laboratory to solve the transfer equation at each pixel location. The specific Monte Carlo solution method used in *Radiance* is described in Ward et al. 1988. The *Radiance* software was originally developed as a tool for illumination design, but has gained wide usage as a computer graphics image synthesis package. Because it was developed as a design tool, the output of *Radiance* has been validated by physical measurements, and by comparisons with other software packages written to calculate illumination (Grynberg, 1989).

One of the useful features of *Radiance* is that, unlike many other computer graphics software packages, it requires physically feasible definitions of the bidirectional reflection distribution functions ρ_{bd}. *Radiance* uses the specular-like plus diffuse-like model for reflectance which is common in radiative transfer. The specular-like reflectance is modelled as a Gaussian function centered around the mirror direction, with the spread of the distribution specified by a "surface roughness" parameter. The diffuse-like reflectance is modelled as ideal Lambertian. *Radiance* uses "texture" maps (more commonly referred to as "bump" maps in graphics literature) to define perturbations of the surface normal to simulate larger scale surface roughness (such as the bumps on the skin of an orange). Within this framework, *Radiance* can accommodate retroreflectance. The retroreflective surface is defined as a specular-like (i.e. Gaussian) reflectance with a bump map which always turns the surface normal towards the viewer. In effect, the "mirror" direction is always back in the direction of the viewer. The result is that the value of ρ_{bd} is calculated by the following equation by *Radiance*.

$$\rho_{bd}(\theta_o,\phi_o;\theta_i,\phi_i) = \rho_s \exp(-\delta^2/4\alpha^2)/4\pi\alpha^2\cos\theta_i \qquad (6)$$

where δ is the angle between the view direction (θ_o,ϕ_o) and the direction of incident radiation (θ_i,ϕ_i), and α is the parameter specifying "surface roughness."

Radiance also requires physically feasible definitions of light sources. Sources are modelled as finite surfaces, rather than as points. The emitted radiance across each light source surface can vary spatially. The directionality of the emitted radiance may also vary. One way the directionality can be specified is giving a light source direction, and the size of the cone angle ξ around that direction. Another way is to give a list of relative light source intensities for directions specified in spherical coordinates.

For a given viewpoint, view frustum and image resolution RxQ (R pixels by Q pixels), *Radiance* returns a radiance value for each pixel assuming an infinitesimal pinhole and infinitesimal pixels (i.e. only one location (x_p,y_p) is considered for each pixel). The average radiance over each pixel can be calculated by calculating an image at a higher resolution MRxMQ. At this resolution each pixel is jitter sampled -- i.e. the location (x_p,y_p) for each pixel is chosen randomly. An RxQ resolution image with average pixel radiance is formed by filtering down the high resolution MRxMQ image. Using this jittering and filtering technique then, I_{pixel} as given in Eq. (1) is calculated by *Radiance*.

The *Radiance* package does not have an explicit mechanism for integrating over a finite pinhole. In this project we use the following approximation for Eq. 4:

$$E_i(\theta_{p,i},\phi_{p,i}) \cong I_{i,ave}(\theta_{p,i},\phi_{p,i})\cos\theta_{p,i}\tau\Omega_{pinhole} \qquad (7)$$

where:

$I_{i,ave}(\theta_{p,i},\phi_{p,i})$ is the average radiance incident through the pinhole obtained by sampling the radiance through many points on the pinhole.

$\Omega_{pinhole}$ is the solid angle subtended by the pinhole

$I_{i,ave}(\theta_{p,i},\phi_{p,i})$ is found by taking the weighted average of the radiances calculated using several different positions for the infinitesimal pinhole, taking into account the shift in pixel registration when the pinhole is moved. We chose a sampling pattern which requires only integer pixel shifts, and which samples the pinhole area relatively uniformly. The weight associated with each sample is equal to the fraction of the pinhole area that sample represents.

$\Omega_{pinhole}$ in Eq. (6) is equal to the area of the pinhole projected in the direction of the sensor pixel, divided by the distance squared from the sensor pixel to the pinhole. For a sensor plane parallel to the pinhole, $\Omega_{pinhole}$ can be expressed in terms of the pinhole size d and the focal distance f:

$$\Omega_{pinhole} = \frac{\frac{\pi d^2}{4}\cos\theta_{p,i}}{\left(\frac{f}{\cos\theta_{p,i}}\right)^2} \tag{8}$$

Combining Eqs. (7) and (8) gives:

$$E_i(\theta_{p,i},\phi_{p,i}) \cong I_{i,ave}(\theta_{p,i},\phi_{p,i})\cos^4\theta_{p,i}\,\pi d^2\tau/4f^2 \tag{9}$$

The value of E_{pixel} in Eq. (3) is found by calculating values of $I_{i,ave}(\theta_{p,i},\phi_{p,i})$ from images in which several samples per pixel were taken.

For our initial implementation we considered averaged values for a single wavelength band. The method for producing a simulated captured image using *Radiance* is summarized in the following pseudocode:

```
/* Find Average Pixel Radiances for X Pinhole Locations */
For each pinhole sample location X
        {
        Calculate the array of radiances I[X][RM][RN];
        Filter the result of the supersampled image down to I[X][M][N];
        }
/* Find Composite Image for Radiance Averaged over the Pixel and the Pinhole */
I_AVE = 0;
For each filtered image X
        {
        Shift I[X] so that pixels line up with image centered around pinhole;
        I_AVE += weight[X]* I[X];
        }
/* Calculate Average Energy/Area  E from Average Radiance I_AVE*/
/* And Compute Gray Scale G from E */
For each pixel [0][0] to [M-1][N-1]
        {
        E[m][n] = I_AVE[m][n]*cos^4θ[m][n]*πd^2τ/4f^2;
        If  (E[m][n] < E_saturation)
                G[m][n] = K*(E[m][n])^γ+G_o;
        else G[m][n] = G_max;
        }
```

4. A Comparison of Captured and Synthetic Images

In this initial investigation, we compared a series of synthetic images generated by increasingly physically accurate methods to images captured by an existing vision system. Our goal was to examine whether there were meaningful differences in the accuracy of the various synthetic images.

The vision system of the type described in section 2 was used with D = 0.48 m, f = 6.75 mm, d = 0.1 mm and w = 2.54 cm. The illumination system consisted of N=12 AlGaAs LEDs (Hewlett Packard model HLMP-8104), which are designed to concentrate the luminous flux into a cone of $\xi = 7$ degrees. The typical relative angular intensity distribution for the LEDs is shown in Fig. 6. The LEDs have a peak intensity at a wavelength of 650 nm. The LEDs were chosen as low cost, low power consumption, long life sources with spectral characteristics matching the imaging sensor. The imaging sensor was a Texas Instruments CCD TC-211, the output of which was sampled at 4 MHz using a Motorola MC 101319, an 8-bit analog-to-digital flash converter. 3M Scotchlite Reflective Sheeting (#3870), a commercially available retroreflective material, was used as a retroreflective background.

The camera energy/area to gray scale transfer function defined in Eq. (5) was calibrated by shining one of the LEDs directly into the camera from distance D, and recording the gray scale values obtained by averaging over the 35 brightest pixels for various exposure times τ. The values obtained were K = 33,844, $\gamma = .85$, $G_o = 12$ and $G_{max} = 161$.

Two images captured by the system were used for comparison -- an image of the plain retroreflective background and an image with a shiny stainless steel washer. The images were captured with low ambient light. The captured images are shown in Figs. 7 and 12. (Note: Figs. 7-14 can be found on the two 35 mm slides accompanying this paper.)

For comparison with the captured image of the plain retroreflective background, the following series of synthetic images were produced:

Fig. 8: Background modelled as Lambertian with $\rho_d = 1$, camera modelled with infinitesimal pinhole and light source modelled as 7 degree cone.

Fig. 9: Background modelled with ρ_{bd} given in Eq. (6), with $\rho_s = .086$ and $\alpha = .00612$ (parameters chosen to fit data for Scotchlite), camera modelled with infinitesimal pinhole and light source modelled as 7 degree cone.

Fig. 10: Background modelled with ρ_{bd} given in Eq. (6), with $\rho_s = .086$ and $\alpha = .00612$, camera modelled with finite pinhole and light source modelled as 7 degree cone.

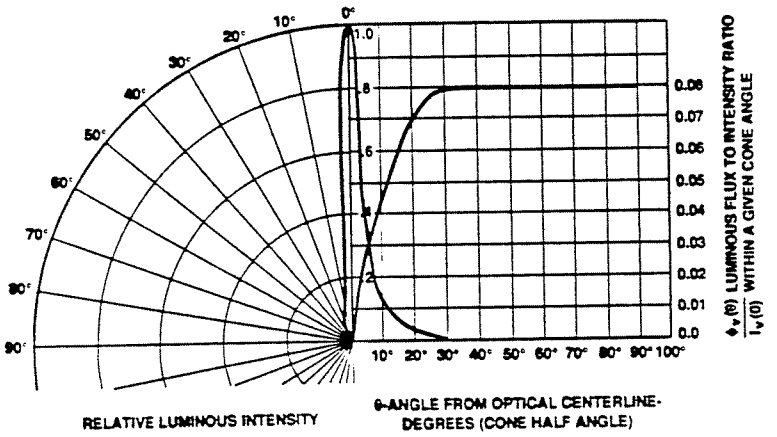

Figure 6: Relative variation of source intensity for the HP 8104 LEDs.

Fig. 7 Fig. 8 Fig. 9

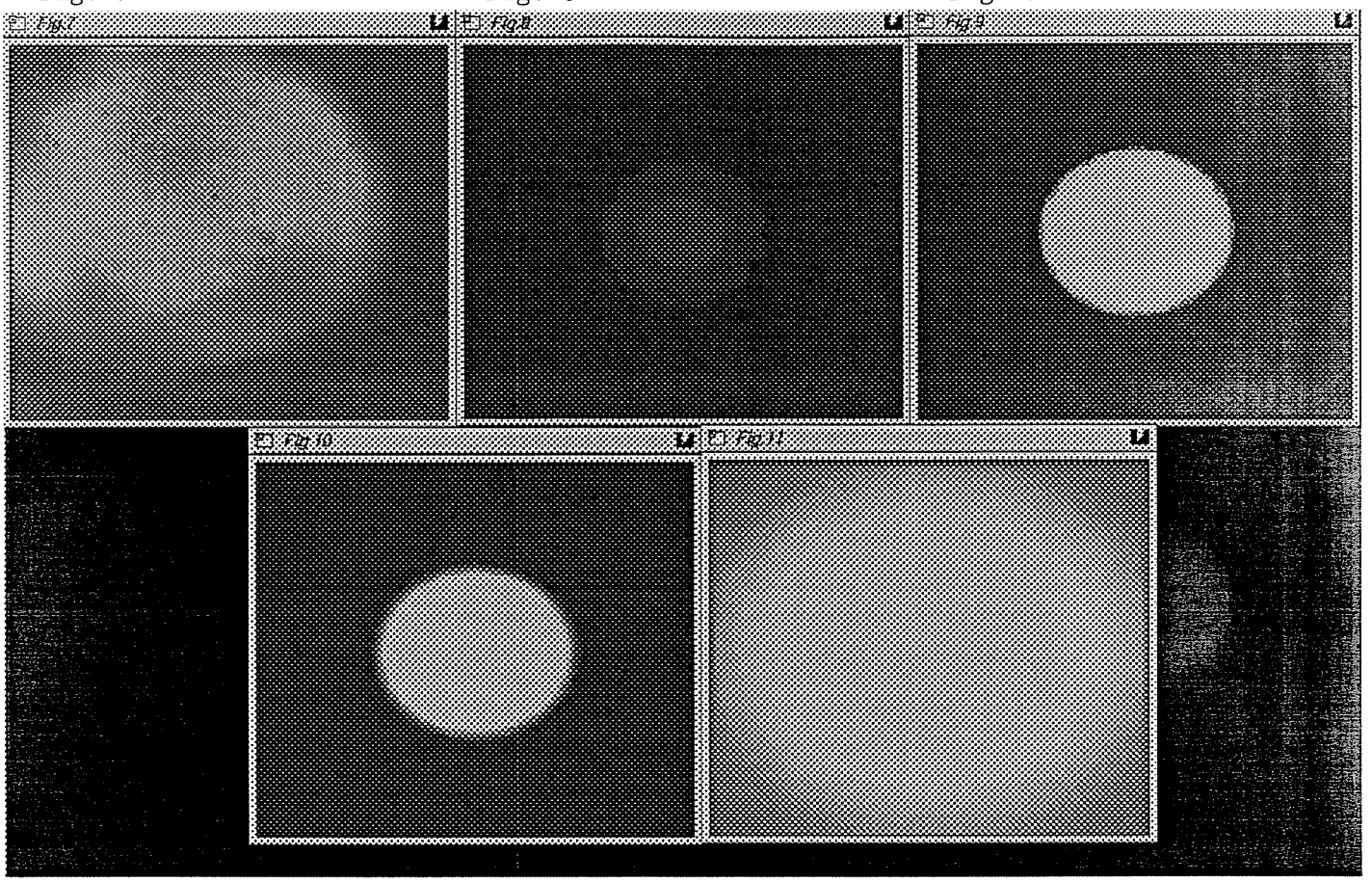

Fig. 10 Fig. 11

(Figures on 35mm slide #1)

Fig. 12 Fig. 13 Fig. 14

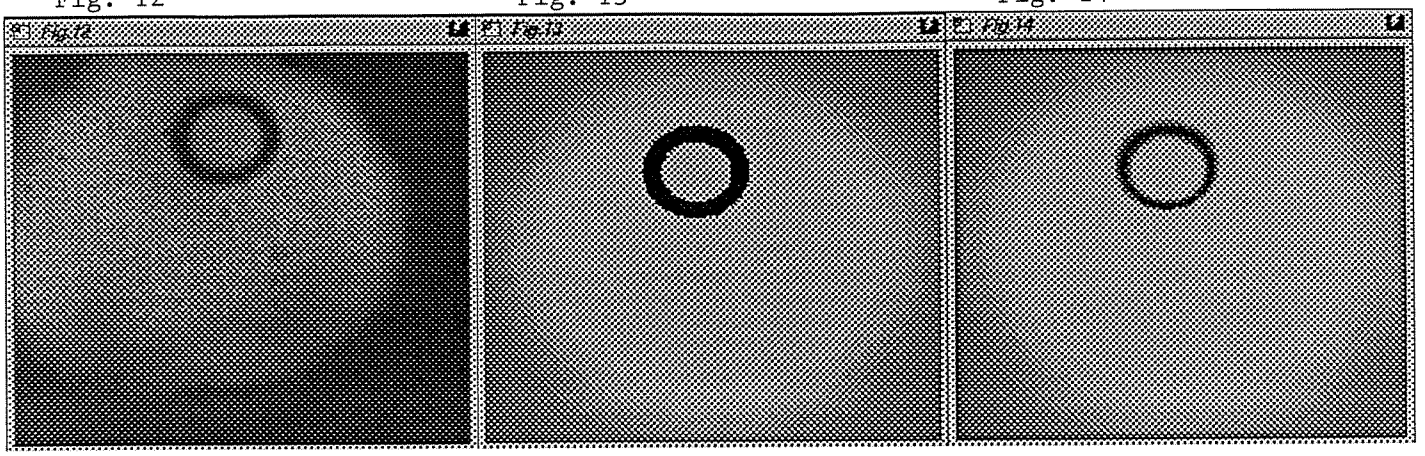

(Figures on 35mm slide #2)

Fig. 11: Background modelled with ρ_{bd} given in Eq. (6), with $\rho_s = .086$ and $\alpha = .00612$, camera modelled with finite pinhole and light source modelled with the directional distribution shown in Fig. 6.

Figures 8 to 11 represent increasingly accurate simulations of the image. Figure 8 is the grade of output that would be obtained using a standard CAD package. Clearly the image, which is nearly black, is useless for camera system design. In Fig. 9 the use of the correct retroreflectance results in realistic gray scale values, but the illuminated area is too small, and too sharply defined. In Fig. 10, the averaging over the finite pinhole removes the sharp edges, but the illuminated area is clearly still too small. Finally, using the more accurate directional light source distribution in Fig. 11 results in a larger illuminated area.

For comparison with the image with the washer two synthetic images were produced. In each the washer is modelled as ideal specular (i.e. perfectly smooth) with a reflectance of $\rho_s = .8$.

Fig. 13: Background modelled with ρ_{bd} given in Eq. (6), with $\rho_s = .086$ and $\alpha = .00612$, camera modelled with infinitesimal pinhole and light source modelled with the directional distribution shown in Fig. 6.

Fig. 14: Background modelled with ρ_{bd} given in Eq. (6), with $\rho_s = .086$ and $\alpha = .00612$, camera modelled with finite pinhole and light source modelled with the directional distribution shown in Fig. 6.

Comparing Figs. 13 and 14 to the captured image Fig. 12 shows that averaging over the finite area of the pinhole is important in accurately simulating the appearance of the edge of the washer, and the contrast between the washer and the background.

While the synthetic images show that the correct reflectance distribution, light source distribution and pinhole model are critical in accurately simulating the captured images, none of the synthetic images matched the captured images perfectly. The illuminated area in the captured images Figs. 7 and 12 is more sharply defined than in Figs. 11 and 14. This may be because a Gaussian does not adequately model the sharp fall-off in the retroreflectance, and that another function should be used. The geometric alignment of the camera system, which resulted in the captured image being off-center, needs to be simulated more accurately. The retroreflective coating used was a flexible sheet that may not have been perfectly smooth, possibly causing some of the irregularities in the illuminated area. There was a subtle pattern on the Scotchlite sheeting which is visible in the image which needs to be modelled in the simulation. Also, the Scotchlite has a specular sheen which should be modelled. The washer in Fig. 14 does not have the same shape as in the captured image. This may be due to the precise placement of the washer, or because the reflectance of the washer needs to be modelled more accurately.

5. Conclusions and Future Work

Synthetic images have the potential to be useful in designing computer vision hardware/software systems. We have presented a methodology for generating physically accurate synthetic images for simulating the images captured for a computer vision system. We have shown some preliminary comparisons that indicate physically accurate image synthesis methods, rather than the synthesis methods used with standard CAD packages, are necessary to simulate captured images.

In the next phase of comparisons between captured and simulated images we will consider the reflectance modelling and geometric alignment issues mentioned in Section 5. We will go on to test images of many more objects. We will consider a variety of ambient lighting conditions, rather than simply the effect of direct lighting by the vision system itself. Rather than just visually comparing the images we will compare the performance of image processing algorithms on the synthetic and captured images. Once we have completed the validation of the synthetic imaging process, we will go on to use this process to test various intrinsic hardware design parameters, and to develop a template design methodology for feature matching.

6. Acknowledgements

This work was funded by the National Science Foundation under Presidential Young Investigator Grants #8958383 and #9058389. We would like to thank Robert Blenis and Shankar Janakiraman for their help in using the vision system, and Charles Patterson for his help in using the *Radiance* software.

7 References

Chen, C.-H. and Mulgaonkar, P. G., 1991, "CAD-Based Feature Utility Measures for Automatic Vision Programming," IEEE Workshop on Directions in Automated CAD-Based Vision, Maui Hawaii, IEEE Computer Society Press.

Chen, S.E., Rushmeier, H.E., Miller, G. and Turner, D., 1991,"A Progressive Refinement Multi-Pass Method for Global Illumination," *Computer Graphics,* V. 25, N. 4, pp 165-174.

Cook, R.L., Porter, T. and Carpenter, L., 1984,"Distributed Ray Tracing," *Computer Graphics*, V. 18, N. 3, 137-145.

Cowan, C. 1991, "Automatic Camera and Light-Source Placement Using CAD Models," IEEE Workshop on Design in Automatic CAD-Based Vision, Maui Hawaii, IEEE Computer Society Press.

Gagalowicz, A. 1990, "Collaboration Between Computer Graphics and Computer Vision," in *Scientific Visualization and Graphic Simulation*, ed. by D. Thalmann, pp. 233-248.

Goral, C.M., Torrance, K.E., Greenberg, D.P. and Battaile, B. "Modeling the Interaction of Light Between Diffuse Surfaces," *Computer Graphics*, V. 18, N. 3, pp. 213-222.

Grynberg, A., 1989, "Validation of Radiance," Lawrence Berkeley Laboratory, Applied Sciences Division, Lighting Systems Research Group, Report #LBID 1575.

Lee, K.-M., 1991a, "Flexible Part-Feeding System for Machine Loading and Assembly, Part I - A State-of-the-Art Survey," *International Journal of Production Economics*, to appear December 1991.

Lee, K.-M., 1991b, "Flexible Part-Feeding System for Machine Loading and Assembly, Part I I- A Cost Effective Solution" *International Journal of Production Economics*, to appear December 1991.

Lee, K.-M.,. Blenis, R., Yutkowitz, S., Li, D.-R., and Motaghedi, P., 1991, "A Low-Cost Flexible Part-Feeding System for Machine Loading and Assembly" Final Report to Ford Motor Company, General Motors Corporation, the Georgia Tech Materials Handling Research Center, and the National Science Foundation, TR-91-06.

Lee, K.-M. and Janakiraman, S.,1991, "A Real-Time Part-Presentation Algorithm Using Retroreflective Vision Sensing" submitted to Vision Interface 1992.

Kajiya, J.T., 1986, "The Rendering Equation," *Computer Graphics*, V. 20, N. 4, pp. 143-150.

Meyer, G. W., Rushmeier, H.E., Cohen, M.F., Greenberg, D.P. and Torrance, K.E., 1986, "An Experimental Evaluation of Computer Graphics Imagery," *ACM Transactions on Graphics*, V. 5, N. 1, pp. 30-50.

Nishita, T. and Nakamae, E., 1985, "Continuous Tone Representation of Three Dimensional Objects Taking Account of Shadows and Interreflections," *Computer Graphics*, V. 19, N.4 pp. 23-30.

Nakamae, E., Kaneda, K., Okamoto, T., and Nishita, T., 1990, "A Lighting Model Aiming at Drive Simulators," *Computer Graphics*, V24, N4, August, pp. 395-404.

Siegel, R. and Howell, J.R., 1981, *Thermal Radiation Heat Transfer,* Hemisphere, Washington, DC.

Sillion, F.X., Arvo, J.R. and Westin, S.H. and Greenberg, D.P., 1991, "A Global Illumination for General Reflectance Distributions," *Computer Graphics,* V. 25, N. 4, pp. 187-198.

Tsai, R.Y. 1987 "A Versatile Camera Calibration Technique for High Accuracy 3-D Machine Vision Metrology Using Off-the-Shelf TV Camera and Lenses," IEEE Robotics and Automation, Vol. RA-3, N. 4, pp. 323-344.

Tumblin, J.T. and Rushmeier, H. E., "Tone Reproduction for Realistic Computer Generated Images," Georgia Tech GVU Center Tech Report -- GVU-91-13.

Ward, G.J, Rubinstein, F.M. and Clear, R.D., 1988, "A Ray Tracing Solution for Diffuse Interreflections" *Computer Graphics*, V. 22, N. 4, pp. 85-92.

Wu, C. K., Cheatham, J.B., Lin, Y.H. and Cleghorn, T.F., 1990, "Computer Graphics Modelling for Simulating and Testing Robot Vision Systems," *International Journal of Modelling and Simulation,* V10, pp. 67-70.